Available online at www.sciencedirect.com
SCIENCE DIRECT®
Journal of the European Ceramic Society 25 (2005) 681–693
www.elsevier.com/locate/jeurceramsoc

Thermodynamic assessment of the system ZrO_2–CaO–MgO using new experimental results Calculation of the isoplethal section MgO·CaO–ZrO_2

S. Serena*, M. A. Sainz, S. de Aza, A. Caballero

Instituto de Cerámica y Vidrio, C.S.I.C., Campus de Cantoblanco, 28049 Madrid, Spain

Received 28 November 2003; accepted 8 February 2004
Available online 19 June 2004

Abstract

The system ZrO_2–CaO–MgO offers the possibility of obtaining different types of advanced materials from mixtures of ZrO_2 with a natural raw material such as dolomite. The development of these promising materials requires the determination of the system's MgO·CaO–ZrO_2 isoplethal section. The aim of this paper is to carry out the thermodynamic calculation of the system, and especially the isoplethal section mentioned, by means of Calphad methodology.

In this sense, the thermodynamic description of the ZrO_2–CaO–MgO system and its lower order subsystems was achieved and a set of self-consistent parameters reproducing most of the experimental data was obtained. The approach used makes the theoretical estimation of the phase diagrams possible, even in regions with limited or nonexistent experimental information, as is the case of the low temperature range in the ternary system studied.

Keywords: Thermodynamic modeling; Phase equilibria; Phase diagrams; CaO–MgO–ZrO_2

1. Introduction

Ceramic materials with important advanced applications are included in the ZrO_2–CaO–MgO system. The well-known mechanical and electronic properties of the materials based on total or partially stabilized cubic or tetragonal zirconia have led to their widespread use as structural materials,[1] solid-state electrolytes,[2,3] and thermal barrier coatings.[4] At the present time, the development of nanostructured materials based on ZrO_2 is an increasing field[5–8] due to the special mechanical properties of nanocrystalline zirconia-based ceramic.[9,10] Besides this, nanocomposites of MgO/$CaZrO_3$ have promising properties too. In fact, the characteristic behavior of mechanibility and quasiplasticity for MgO/$CaZrO_3$ dense-nanocomposites has been recently pointed out.[11] Also porous-nanocomposites have been studied for applications such as hot gas filter materials[12] or fluid flow filters (industrial waste, beverages, etc), light-weight structural components, high-temperature insulators or membrane supports.[13] Moreover, the $CaZrO_3$ phase doped with In_2O_3[14] presents excellent gas sensibility so the application of porous composites of MgO/$CaZrO_3$ as a selective methane sensor is a real application recently taken into account.[15]

The ZrO_2–CaO–MgO phase diagram is of fundamental importance to efficiently define the processing conditions for obtaining advanced ceramic materials and the subsequent treatments to obtain optimal engineering properties. In this sense, the development of nanostructured materials makes it necessary to understand the system at lower temperatures, because of their special/characteristic processing conditions.

Another important fact is that materials based on ZrO_2 or MgO/$CaZrO_2$ can be obtained in the ZrO_2–CaO–MgO system using a low-cost natural raw material such as dolomite ($MgCa(CO_3)_2$), so the knowledge of the system's MgO·CaO–ZrO_2 isoplethal section is a fundamental requirement for taking advantage of this possibility.

There are few experimental data of the system between 1220 and 1700 °C, and the liquidus surface[16–18] while two thermodynamic assessments of the system have been reported,[19,20] as is indicated in the bibliography. In a previous work, the present authors provided new experimental information between 1600 and 1750 °C, comparing

* Corresponding author.
E-mail address: serena@icv.csic.es (S. Serena).

0955-2219/$ – see front matter © 2004 Elsevier Ltd. All rights reserved.
doi:10.1016/j.jeurceramsoc.2004.02.011

the results with those emerging from the previous thermodynamic calculations.

In the present work, CALPHAD (CALculation of PHAse Diagrams) methodology is applied to the calculation of the ZrO_2–CaO–MgO system. The CALPHAD approach involves the thermodynamic model for the molar Gibbs free energy (G) of various phases in the system. The evaluation of the necessary parameter for describing the G of the phases and the calculation of the diagrams was made by using a computerized optimization program that is available in the Thermo-Calc databank.[21]

The first objective is to evaluate the phase diagrams of the MgO–CaO, ZrO_2–CaO, and ZrO_2–MgO binary systems by obtaining a thermodynamic description of these systems. This description will be combined and then the properties of the ZrO_2–CaO–MgO system will be evaluated by considering new experimental information. Finally, the phase relations will be established for a wide temperature range through thermodynamic calculations. The liquidus surface, and the MgO–$CaZrO_3$ and MgO·CaO–ZrO_2 isoplethal sections will be calculated.

One of the main advantages of the Calphad technique is that it provides insight into the thermodynamics in regions with scant or even no experimental information with some certainty. In this sense, one of the aims of this work is to provide a theoretical description of the low temperature region of the system, through the calculation of the ternary phase diagram, which is useful in guiding experimentation in this problematic area.

2. Phase diagram information

2.1. MgO–CaO system

There are many experimental data related to the MgO–CaO system,[22–26] but the experimental phase diagram proposed by Doman[26] is the most generally accepted. The simplicity of the system, with only one invariant eutectic point and limited solid solutions between the end members, has proved useful as a prototype system for evaluating the accuracy of several approximations for predicting state diagrams in various thermodynamic calculations.[27,28]

The experimental data for the liquid line adopted in our optimization were those published by Doman.[26] For the solid solution of MgO in CaO the data proposed by Longo and Podda[29] and Henney and Jones[30] are allocated a high weight. For the solid solution of CaO in MgO, the higher weight was attributed to what was reported by Doman[26] and Longo and Podda.[16]

2.2. ZrO_2–CaO system

There are really a lot of experimental data related to this system and a very exhaustive revision is collected in a thermodynamic approach by Du et al.[31]

The ZrO_2–CaO system presents an intermediate compound $CaZrO_3$ stable up to 2365 °C. The existence of another two intermediate compounds Φ_1 ($CaZr_4O_9$) and Φ_2 ($Ca_6Zr_{19}O_{44}$) have been established for the system, but their range of stability is currently a controversial question. In this paper the stability of the ϕ_1 and ϕ_2 phases was considered, according to what was proposed by Hellman and Stubican[32] and Yin and Arget[33] so that only two compounds have been considered as stable and included in the calculation: $CaZrO_3$ and ϕ_2 ($Ca_6Zr_{19}O_{44}$). The system presents two invariant eutectic points (Liquid → c-ZrO_2 + $CaZrO_3$ and Liquid → CaO + $CaZrO_3$) and eutectoid points for the decomposition of c-ZrO_2, t-ZrO_2, and Φ_2 phases. The solid solutions of CaO in the c-ZrO_2 and t-ZrO_2 phases is considerable while the solid solutions in the CaO phase are very low and even negligible in the case of the m-ZrO_2, $CaZrO_3$, and Φ_2 phase.

The experimental data considered with a high weight were: for liquidus surface those reported by Stubican and Ray,[34] Traverse and Foex,[35] and Noguchi et al.;[36] for the c-ZrO_2 and t-ZrO_2 compatibility field those reported by Stubican and Ray,[34] Garvie,[37] Stringer,[38] Duran et al.,[39] and Yin and Arget;[33] and for the c-ZrO_2 and $CaZrO_3$ compatibility field those proposed by Stubican and Ray,[34] Duran et al.,[39] Strickler,[40] Cocco,[41] Tien Subbarao,[42] and Nishimo.[43] For the solidus CaO-rich region of the system, the data provide by Noguchi et al.[36] were allocated a high weight.

2.3. ZrO_2–MgO system

As in the case of the ZrO_2–CaO system, there are many experimental data related to the ZrO_2–MgO system, but the experimental system proposed by Grain[44] is the most generally accepted. The existence of intermediate phases such as $Mg_2Zr_5O_{12}$[45] or $MgZr_6O_{13}$[46] has also been considered for the system, but the metastable nature of these phases is generally admitted nowadays. This system presents an invariant eutectic point (Liquid → c-ZrO_2 + MgO) and two eutectoid points for the decomposition of c-ZrO_2 and t-ZrO_2 phases. The solid solutions of MgO in the c-ZrO_2 and t-ZrO_2 phases is considerable, while the solid solutions in MgO and m-ZrO_2 phase are negligible.

The experimental data adopted in this optimization for the liquidus and the eutectic points of the system were those reported by Sim and Stubican,[47] Zhirnova,[48] and Ebert and Cohn.[49] For the extension of the tetragonal-ZrO_2 and cubic-ZrO_2, cubic-ZrO_2 and $Halita_{MgO}$ two-phase regions and the eutectoid point (cubic-ZrO_2 → tetragonal-ZrO_2 + $Halita_{MgO}$), the data published by Grain,[44] Sim and Stubican[47] and Duran et al.[50] and Yin and Arget[33] are attributed the highest weight; for the decomposition of the tetragonal phase the data of Sim and Stubican,[47] Duran et al.[50] are attributed the higher weight and for the subsolidus MgO-rich region of the system, the data reported by Grain[44] have been considered with a high weight.

2.4. ZrO_2–CaO–MgO pseudo-ternary system

There is really little experimental information on the system ZrO_2–CaO–MgO. The first systematic experimental study was that published in 1978 by Longo and Podda[16] who established a first version of the isothermal sections of 1200–1700 °C. Their principal conclusions were that no ternary compound is stable in the system and that cubic zirconia exists with a solid solution of CaO and MgO simultaneously. The latter means that CaO and MgO can replace each other in the cubic zirconia without any structural variation. A more exhaustive determination of the sections of 1220 and 1420 °C was carried out by Hellman and Stubican.[17] These authors include the ϕ_1 and ϕ_2 phases in the ZrO_2–CaO system, and so that is the isothermal section of 1220 °C in the ternary system.

The only experimental investigations on the liquidus surface of the ternary system were reported by de Aza et al.[18] in an experimental study on the CaO–MgO–ZrO_2–SiO_2 quaternary system. Data about the temperature of fusion and the eutectic point of the system MgO–$CaZrO_3$ are published in this work.

Two groups have studied the thermodynamic determination of the ZrO_2–CaO–MgO system, and its binary systems. In 1992 Du et al.[19] published the first thermodynamic evaluation of the ternary system by extrapolating the MgO–CaO, ZrO_2–CaO, and ZrO_2–MgO systems they had previously calculated on the basis of the Bonnier equation. These authors published the isothermal sections calculated for 1220, 1420, and 1700 °C, and the liquidus surface of the system. Their calculations are consistent with the experiments reported by Hellman and Stubican[17] for 1420 °C but not for 1220 °C, or for those obtained by Longo and Podda[16] for 1700 °C. The principal discrepancy was due to the presence of MgO and CaO, cubic-ZrO_2, and $CaZrO_3$ two-phase regions in the calculations of Du et al.,[19] which was not considered in the experimental results published previously, but was needed to complement the phase rule. On the other hand, the liquidus surface calculated by Du et al. was not consistent with the data for the liquidus published for the MgO–$CaZrO_3$ subsystem by de Aza et al.[18] and the presence of an unusual eutectic point when a small amount of CaO was added to the ZrO_2–MgO system reduces the confidence in the liquidus surface calculated by those authors.

The latest thermodynamic calculation of the system, linked to an experimental study of the isothermal sections of 1250, 1300, 1400, and 1500 °C, was reported by Yin and Arget.[20] By extrapolating their own calculated binary systems on the basis of the Muggianu et al.[51] equation, they published isothermal sections between 1250 and 1500 °C, the MgO–$CaZrO_3$ subsystem and the liquidus surface of the system. The isothermal sections published were consistent with their own experimental data and the liquidus surface of the MgO–$CaZrO_3$ system was in accordance with the experimental data of de Aza et al.[18]

The scant and, in some cases, contradictory experimental information on ZrO_2–CaO–MgO lead the present authors to contribute more experimental data to the system at high temperatures. In a previous study, the experimental determination of the isothermal sections of 1600, 1700, and 1750 °C was carried out.[52] These new data include boundaries between all the compatibility fields on the isothermal sections and the composition of the cubic-ZrO_2 solid solution of the cubic-ZrO_2–$CaZrO_3$–MgO tie triangle for the three temperatures.

The experimental data reported by Yin and Arget[20] and Serena et al.[52] were considered during the optimization.

3. Thermodynamic model

3.1. Lattice stabilities

The stable solid form of pure CaO and MgO is halite, while three stable forms c-ZrO_2, t-ZrO_2, and m-ZrO_2 are possible for pure ZrO_2 as a function of temperature. The lattice stability of the phases employed during the present calculation are listed in Table 1. Lattice stabilities for the stable forms are those proposed by Dinsdale[53] while the metastable forms considered are those reported by Yin and Arget.[20]

3.2. Thermodynamic modeling of binary compounds

Two binary compounds were considered in the calculation: $CaZrO_3$ and ϕ_2 ($Ca_6Zr_{19}O_{44}$). Although the presence of solid solutions of MgO and CaO in the $CaZrO_3$ phase has recently been pointed out,[52] there is not sufficient structural information for a consistent thermodynamic description of this situation. In any event, the low values reported for this solid solution allow the treatment of $CaZrO_3$ as a binary compound as a first approach.

Because the enthalpy increment has been measured in a wide temperature range, the mole Gibbs free energy of $CaZrO_3$ and ϕ_2 are expressed by the following:

$$^{\circ}G = A + BT + CT\ln T + DT^2 + ET^{-1}$$

Here *A*, *B*, *C*, *D*, and *E* are parameters to be optimized. The value of these parameters calculated by Yin and Arget[20] for the $CaZrO_3$ provides a description of *G* for the phase consistent with their own experimental measurement and with the thermodynamic properties collected in thermodynamic tables for this phase. Also a good match was found between the *G* calculated by Yin and Arget[20] and the mean heat capacity of the ϕ_2 phase estimated by these authors from measurement by drop calorimetry. Thus, the Gibbs free energy function proposed by Yin and Arget[20] for the $CaZrO_3$ and ϕ_2 phases will be adopted in this calculation.

Table 1
Summary of lattice stabilities of ZrO_2, CaO, and MgO employed in the present assessment

ZrO_2 (monoclinic)
298.15 – 3500: $-1126367.62 + 426.0761T - 69.6218T\ln(T) - 3.7565 \times 10^{-3}T^2 + 702910/T$

ZrO_2 (tetragonal)
298.15–3500: $-1121646.512 + 479.515703T - 78.10T\ln(T)$

ZrO_2 (cubic)
298.15–3500: $-1113681.0 + 491.486437T - 80.0T\ln(T)$

ZrO_2 (halite)
298.15–1478: $-1025305.80 + 391.9331T - 69.6218T\ln(T) - 3.7565 \times 10^{-3}T^2 + 702910/T$
1478–2208: $-1028659.52 + 450.83609T - 78.10T\ln(T)$
2208–3500: $-1077014.722 + 641.362639T - 100.0T\ln(T)$

ZrO_2 (liquid)
298.15–1478: $-1031671.62 + 391.9331T - 69.6218T\ln(T) - 3.7565 \times 10^{-3}T^2 + 702910/T$
1478–2208: $-1035025.34 + 450.83609T - 78.10T\ln(T)$
2208–3500: $-1083380.54 + 641.362639T - 100.0T\ln(T)$

CaO (tetragonal)
298.15–3172: $-560439.72 + 315.22123T - 51.8583T\ln(T) - 1.2193 \times 10^{-3}T^2 - 2.4167 \times 10^{-11}T^3 + 468306.5/T$
3172–6000: $174627.96 - 2001.82115T + 227.015259T\ln(T) - 4.53855 \times 10^{-2}T^2 + 1.17119 \times 10^{-6}T^3 - \cdot 3.48615 \times 10^{8}/T$

CaO (cubic)
298.15–3172: $-560709.74 + 315.22123T - 51.8583T\ln(T) - 1.2193 \times 10^{-3}T^2 - 2.4167 \times 10^{-11}T^3 + 468306.5/T$
3172–6000: $174357.941 - 2001.82115T + 227.015259T\ln(T) - 4.53855 \times 10^{-2}T^2 + 1.17119 \times 10^{-6}T^3 - 3.48615 \times 10^{8}/T$

CaO (halite)
298.15–3172: $-653631.36 + 315.22123T - 51.8583T\ln(T) - 1.2193 \times 10^{-3}T^2 - 2.4167 \times 10^{-11}T^3 + 468306.5/T$
3172–6000: $81436.32 - 2001.82115T + 227.015259T\ln(T) - 4.53855 \times 10^{-2}T^2 + 1.17119 \times 10^{-6}T^3 - 3.48615 \times 10^{8}/T$

CaO (liquid)
298.15–1830: $-585630.85 + 300.654841T - 52.862T\ln(T) - 1.5545 \times 10^{-4}T^2 - 1.89185 \times 10^{-7}T^3 + 489415/T$
1830–2880: $-793806.27 + 1510.9933T - 212.686T\ln(T) + 5.49185 \times 10^{-2}T^2 - 3.789867 \times 10^{-6}T^3 + 51730500/T$
2880–3172: $-4191941.74 + 15458.994T - 1961.24T\ln(T) + 0.4554355T^2 - 2.101933 \times 10^{-5}T^3 + 1.29186 \times 10^{9}/T$
3172–6000: $-663523.92 + 573.648794T - 84T\ln(T)$

MgO (tetragonal)
298.15–1700: $-527182.742 + 298.25357T - 47.4817T\ln(T) - 2.32681 \times 10^{-3}T^2 + 4.50428333^{-8}T^3 + 489415/T$
1700–3100: $-563244.058 + 528.597187T - 78.3772T\ln(T) + 9.7344 \times 10^{-3}T^2 - 8.3033833 \times 10^{-7}T^3 + 8591550/T$
3100–5000: $-79244.3991 - 1409.43369T + 163.674142T\ln(T) + 0.0440095354T^2 + 1.3748963 \times 10^{-6}T^3 - 1.72665403 \times 10^{8}/T$
5000–6000: $-630166.957 + 617.657452T - 84T\ln(T)$

MgO (cubic)
298.15–1700: $-442913.372 + 276.722381T - 47.4817T\ln(T) - \cdot 2.32681 \times 10^{-3}T^2 + 4.50428333^{-8}T^3 + 489415/T$
1700–3100: $-478974.688 + 507.065997T - 78.3772T\ln(T) + 9.7344 \times 10^{-3}T^2 - 8.3033833 \times 10^{-7}T^3 + 8591550/T$
3100–5000: $5024.97090 - 1430.96488T + 163.674142T\ln(T) + 0.0440095354T^2 + 1.3748963 \times 10^{-6}T^3 - 1.72665403 \times 10^{8}/T$
5000–6000: $-545897.588 + 596.126262T - 84T\ln(T)$

MgO (halita)
298.15–1700: $-619428.5 + 298.25357T - 47.4817T\ln(T) - 2.32681 \times 10^{-3}T^2 + 4.50428333 \times 10^{-8}T^3 + 489415/T$
1700–3100: $-655489.82 + 528.597187T - 78.3772T\ln(T) + 9.7344 \times 10^{-3}T^2 - 8.3033833 \times 10^{-7}T^3 + 8591550/T$
3100–5000: $-171490.1591 - 1409.43369T + 163.674142T\ln(T) + 0.0440095354T^2 + 1.3748963 \times 10^{-6}T^3 - 1.72665403 \times 10^{8}/T$
5000–6000: $-722412.7175 + 617.657452T - 84T\ln(T)$

MgO (liquid)
298.15–1700: $-549098.32982 + 275.7246342T - 47.4817T\ln(T) - 2.32681 \times 10^{-3}T^2 + 4.50428333 \times 10^{-8}T^3 + 489415/T$
1700–3100: $-585159.6465 + 506.0682498T - 78.3772T\ln(T) + 9.7344 \times 10^{-3}T^2 - 8.3033833 \times 10^{-7}T^3 + 8591550/T$
3100–5000: $-9110429.749 - 42013.7634T + 5298.548T\ln(T) - 1.301224854T^2 + 5.826260095 \times 10^{-5}T^3 - 3.240374162 \times 10^{9}/T$
5000–6000: $-632664.4682 + 589.23955533T - 84T\ln(T)$

$CaZrO_3$
298.15–3500: $-1811131.76 + 789.36708T - 129.955T\ln(T) - 1.569 \times 10^{-3}T^2 + 1046000/T$

$Ca_6Zr_{19}O_{44}$ (ϕ_2)
298.15–3500: $-25207839.3 + 8221.352T - 1428.24T\ln(T) - 0.10499T^2 + 13800000/T$

The lattice stabilities are defined as $G\text{-}H_{SER}$ where SER stands for stable element reference at 298.15 K. The energy unit used is joule per mole of unit formula.

3.3. Thermodynamic modeling of binary liquid and solid solution phases

No ordering or immiscibility has been observed for the liquid phase of the binary or ternary system considered, so that the liquid phases can be modeled as a substitutional solution.

From their thermodynamic and electric properties, it seem reasonable that all the solution phases in the binary and ternary systems can be described as ionic, the cations and anions being in their simplest forms (Ca^{+2}, Mg^{+2}, Zr^{+4}, and O^{-2}). The structural studies on the MgO–CaO system clearly show that Mg^{+2} and Ca^{+2} can replace each other in the corresponding lattice without generating vacancies. However, substitution of Zr^{+4} by Mg^{+2} and Ca^{+2} in the rich-ZrO_2 phases or substitution of Mg^{+2} and Ca^{+2} by Zr^{+4} in the corresponding lattice defect generation is necessary for maintaining the charge neutrality. Moreover, the defect type can be complex and temperature dependent, as was observed for the ZrO_2–CaO system, and changes from anion vacancies to cation interstitial as the temperature increases. In this sense, it is still not enough to give a clear image of the structures which could be used to account for a sublattice model, so that in order to estimate the diagrams, the substitutional model has still been applied to describe the solid solutions in the present work.

According to the above discussion, the liquid and solid solutions phases in the systems are described by the substitutional model related to the Standard Element Reference, i.e. the enthalpies of the pure elements in their defined reference phase at 298.15 K. The Gibbs free energy is given by the following equation:

$$\Delta G^{i,j}_{\text{phase}}(x,T) = \sum_i x_i \Delta^\circ G^i_{\text{phase}}(T) + RT\sum_i x_i \ln x_i + \Delta G^{\text{xs},i,j}_{\text{phase}} \quad i,j = \text{ZrO}_2, \text{CaO}, \text{MgO} \quad (1)$$

Here x_i is the mole fraction of ZrO_2, CaO, and MgO, and $\Delta^\circ G^i_{\text{phase}}(T)$ is the Gibbs free energy of i in the phase, related to its reference state (shown in Table 1). The second term is the ideal entropy of mixing and the final term in the excess Gibbs free energy, given by:

$$\Delta G^{\text{xs},i,j}_{\text{phase}} = x_i x_j \sum_\nu ({}^\nu L^{0,i,j}_{\text{phase}} + {}^\nu L^{1,i,j}_{\text{phase}} T)(x_i - x_j)^\nu \quad i,j = \text{ZrO}_2, \text{CaO}, \text{MgO} \quad (2)$$

Here ${}^\nu L^{0,i,j}_{\text{phase}}$ and ${}^\nu L^{1,i,j}_{\text{phase}}$ are the parameters to be optimized for each phase considered in the systems and $\nu < 2$.

The similitude between the MgO and CaO makes it possible to describe the solid solution of MgO in CaO and CaO in MgO as a unique phase, called Halite, with a miscibility gap not observed due to the appearance of the liquid phase. The $\text{Halite}_{\text{MgO}}$ and $\text{Halite}_{\text{CaO}}$ represent the rich-MgO halite phase and the rich-CaO halite phase, respectively.

3.4. Thermodynamic modeling of ternary liquid and solid solution phases

The Gibbs free energy of a ternary solution phase is extrapolated from the binary phases on the basis of the Muggianu equation. This equation is in accordance with a symmetrical model that considers the identical contribution of the binary phases to the Gibbs free energy of the ternary phases. According to this equation and in a subregular solution model, the last term of Eq. (1) expands to:

$$\Delta G^{\text{xs}}_{\text{phase}} = \sum_{i,j,i\neq j} x_i \cdot x_j \cdot \left[\sum_{\nu=0,1} ({}^\nu L^{0,i,j}_{\text{phase}} + {}^\nu L^{1,i,j}_{\text{phase}} \cdot T) \cdot (x_i - x_j)^\nu \right]$$

$i, j = \{\text{ZrO}_2, \text{CaO}, \text{MgO}\}$

Other widely used geometrical methods, such as the Kohler equation, have also been used to estimate the ternary system in the present work, but the Muggianu equation has been found to give the best fitting of the experimental information in the present assessment.

In the calculation of the Gibbs free energy for the cubic-ZrO_2 phase with solid solutions of CaO and MgO, it was necessary to include ternary excess parameters to reproduce the experimental data, due to the considerable quantity of both components in the solid phase. The contribution of ternary interactions to the Gibbs free energy in a substitutional solution model is:

$$\Delta G^{\text{xs,ternary}}_{\text{phase}} = x_{\text{ZrO}_2} x_{\text{CaO}} x_{\text{MgO}} ({}^\circ L^{0,\text{ZrO}_2,\text{CaO},\text{MgO}}_{\text{phase}} + {}^\circ L^{1,\text{ZrO}_2,\text{CaO},\text{MgO}}_{\text{phase}} T)$$

Here ${}^\circ L^{0,\text{ZrO}_2,\text{CaO},\text{MgO}}_{\text{phase}}$ and ${}^\circ L^{1,\text{ZrO}_2,\text{CaO},\text{MgO}}_{\text{phase}}$ are the ternary parameters to be optimized for c-ZrO_2 phase in the ternary system.

4. Parameter evaluation and results

The optimization was made using a program called PARROT included in the Thermo-Calc databank system,[21] and considering the experimental data indicated in the preceding section. All equilibria were calculated using the Poly-3 program included in the same software.

The optimization was conducted by minimizing the sum of squares, and repeated until a satisfactory description of most experimental data points was reached, within the claimed uncertainty limits.

4.1. MgO–CaO system

The excess energy coefficients optimized in the present work are shown in Table 2 and the diagram calculated is

Table 2
Excess Gibbs free energy coefficients optimized in the present work for the MgO–CaO, ZrO_2–CaO, ZrO_2–MgO, and ZrO_2–CaO–MgO system

Phase	Reference state		$^{\circ}L^0$	$^{\circ}L^1$	$^1L^1$
			MgO–CaO		
Liquid	MgO (liq.)	CaO (liq.)	4341.70	0	−18766.45
Halite	MgO (hal.)	CaO (hal.)	89446.32	−13.12	−13767.16
			ZrO_2–CaO		
Liquid	ZrO_2 (liq.)	CaO (liq.)	−141241.63	19.44	0
Halite	ZrO_2 (hal.)	CaO (hal.)	−126962.16	0	0
Cubic	ZrO_2 (cub.)	CaO (cub.)	−194982.49	13.97	0
Tetragonal	ZrO_2 (tet.)	CaO (tet.)	−127310.55	0	0
			ZrO_2–MgO		
Liquid	ZrO_2 (liq.)	MgO (liq.)	74079.66	−46.46	−23267.73
Halite	ZrO_2 (hal.)	MgO (hal.)	35148.50	9.15	0
Cubic	ZrO_2 (cub.)	MgO (cub.)	−134674.18	−8.80	0
Tetragonal	ZrO_2 (tet.)	MgO (tet.)	−139670.36	60.20	0
			ZrO_2–CaO–MgO		
Cubic	ZrO_2 (cub.) CaO (cub.) MgO (cub.)		−187702.16	75.00	0

Table 3
Calculated invariant point for the system MgO–CaO

Invariant point	T (°C)	Phase composition (mol% MgO)		
		Liquid	$Halite_{CaO}$	$Halite_{MgO}$
Eutectic: Liquid → $Halite_{CaO}$ + $Halite_{MgO}$	2352	43.36	21.20	93.88

shown in Fig. 1. Table 3 shows the eutectic points calculated for the system. A fair agreement is observed between the diagram calculated and the experimental points generally accepted, except in the CaO-rich region at high temperatures. The disagreement is due to the higher temperatures attributed to the fusion of the pure CaO in the database employed compared with that proposed by some authors.

4.2. ZrO_2–CaO system

The excess energy coefficients optimized in the present work are shown in Table 2 and the complete ZrO_2–CaO phase diagram calculated using the present set of thermodynamic parameters is shown in Fig. 2. Table 4 shows the invariant points calculated for the system. There is a

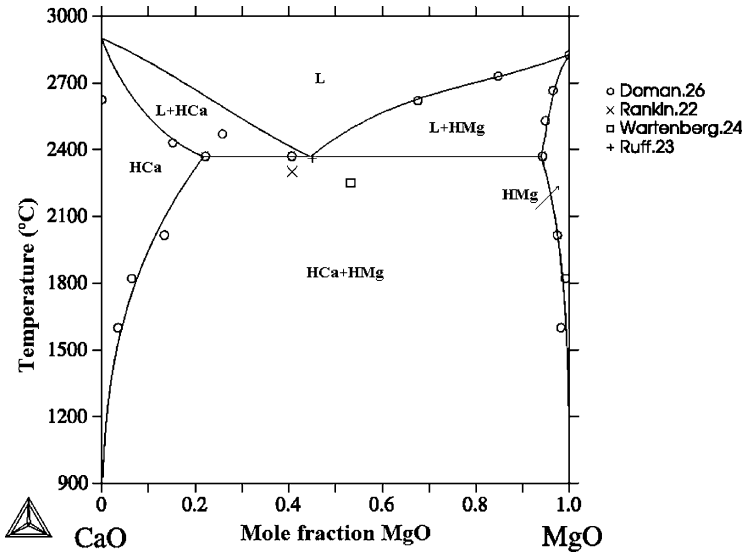

Fig. 1. The optimized phase diagram MgO–CaO. As comparison, the selected experimental data are also shown in the diagram. L=Liquid; HCa=Halita(CaO); HMg=Halite(MgO).

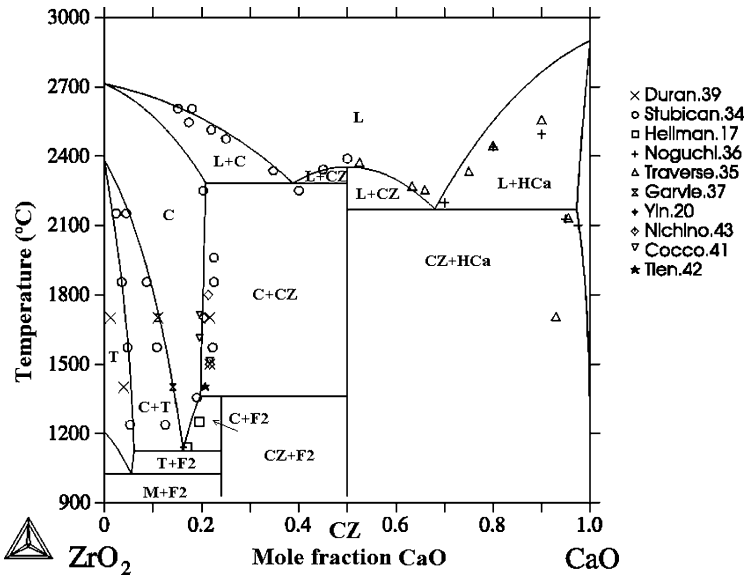

Fig. 2. The optimized phase diagram ZrO_2–CaO. As comparison, the selected experimental data are also shown in the diagram. L=Liquid; C=c–ZrO_2; T=t–ZrO_2; M=m–ZrO_2; HCa=Halita(CaO); CZ=$CaZrO_3$; F2=$Ca_6Zr_{19}O_{44}$.

substantial agreement between the diagram calculated and the reported experimental points, except in the CaO-rich region at high temperatures. Again, the disagreement is due to the higher temperatures attributed to the fusion of the pure CaO in the database used compared to that proposed by some authors. For the rich-ZrO_2 region at low temperatures, there is a lack of experimental information so that this must basically be considered as a theoretical approach.

4.3. ZrO_2–MgO system

The phase equilibrium diagram calculated for the system ZrO_2–MgO calculated by employing the excess energy coefficients optimized in the present work (Table 2) is shown in Fig. 3. The invariant points calculated for the system are shown in Table 5. A good agreement is observed between the calculated diagram and the experimental points for the liquidus and solidus regions and the invariant points of the system.

4.4. ZrO_2–CaO–MgO system

The resulting ternary optimized excess energy coefficients can be observed in Table 2. The liquidus surface, isothermal and isoplethal sections calculated for a complete description of the system as shown in Figs. 4–9 are discussed below.

4.4.1. Liquidus surface calculated for the ZrO_2–CaO–MgO system

The computed projection of the liquidus surfaces of the system is shown in Fig. 4. The three invariant points calculated for the system (named E1, E2, and E3) are indicated in Table 6.

Table 4
Calculated invariant point for the system ZrO_2–CaO

Invariant point	T (°C)	Phase composition (mol% CaO)		
		Liquid	$CaZrO_3$	Cubic
Eutectic: Liquid → Cubic + $CaZrO_3$	2283	38.77	50.00	20.87
		Liquid	$CaZrO_3$	$Halite_{CaO}$
Eutectic: Liquid → $CaZrO_3$ + $Halite_{CaO}$	2169	68.00	50.00	97.24
		Cubic	Tetragonal	Φ_2
Eutectoid: Cubic → Tetragonal + ϕ_2	1122	16.20	6.05	24.00
		Tetragonal	Monoclinic	ϕ_2
Eutectoid: Tetragonal → Monoclinic + ϕ_2	1025	5.53	0	24.00
		Cubic	ϕ_2	$CaZrO_3$
Decomposition: ϕ_2 → Cubic + $CaZrO_3$	1363	19.74	24.00	50.00

Table 5
Calculated invariant point for the system ZrO_2–MgO

Invariant point	T (°C)	Phase composition (mol% MgO)		
		Liquid	$Halite_{MgO}$	Cubic
Eutectic: Liquid → Cubic + $Halite_{MgO}$	2109	50.41	99.00	21.76
		Cubic	$Halite_{MgO}$	Tetragonal
Eutectoid: Cubic → Tetragonal + $Halite_{MgO}$	1406	13.34	99.89	1.92
		Tetragonal	Monoclinic	$Halite_{MgO}$
Eutectoid: Tetragonal → Monoclinic + $Halite_{MgO}$	1128	3.14	0	99.98

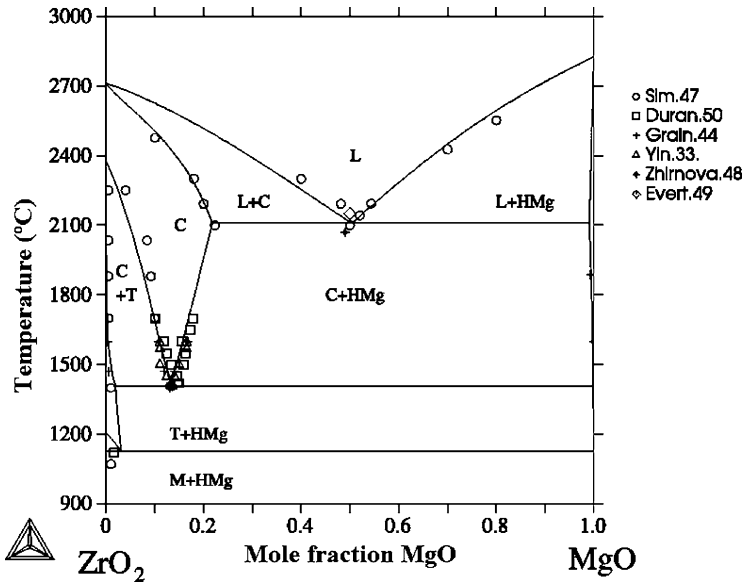

Fig. 3. The optimized phase diagram ZrO_2–MgO. As comparison, the selected experimental data are also shown in the diagram. L=Liquid; C=c–ZrO_2; T=t–ZrO_2; M=m–ZrO_2; HMg=Halita(MgO).

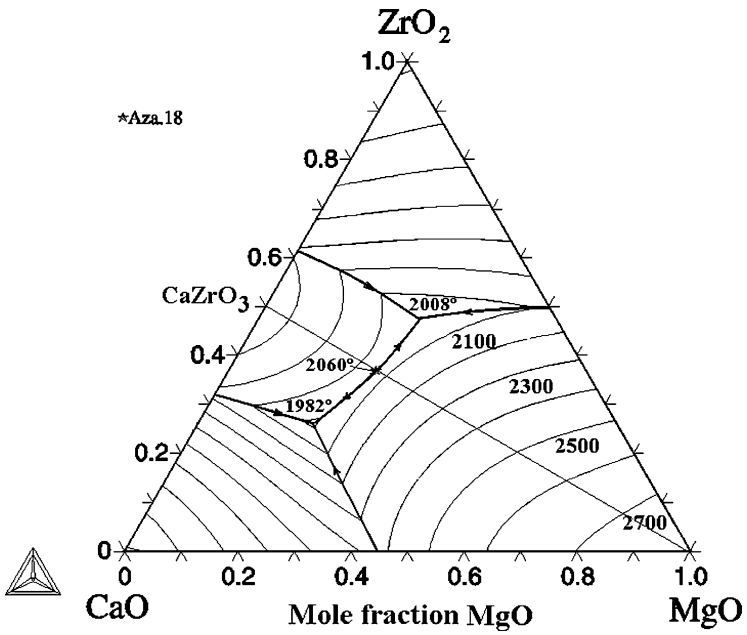

Fig. 4. The liquid surface of the optimized phase diagram ZrO_2–CaO–MgO. As comparison, the selected experimental data are also shown in the diagram.

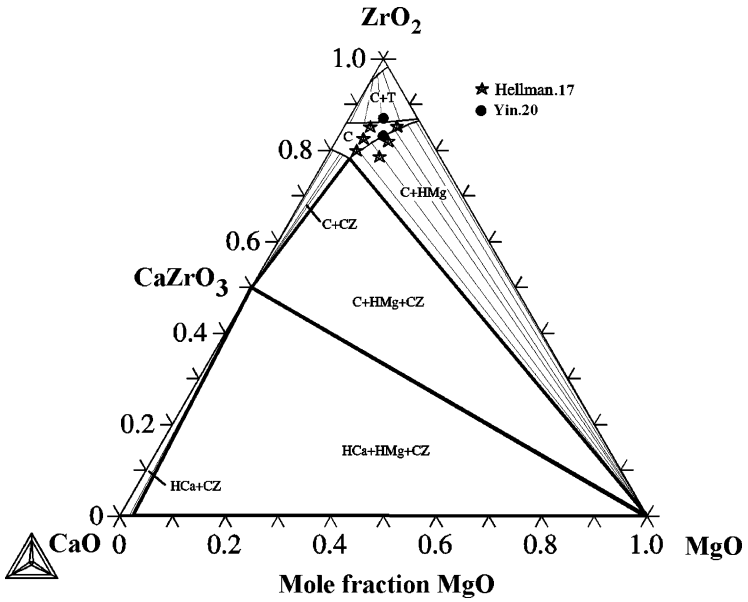

Fig. 5. The isothermal section at 1693 K of the optimized phase diagram ZrO_2–CaO–MgO. As comparison, the selected experimental data are also shown in the diagram. C=c–ZrO_2; T=t–ZrO_2; HCa=Halita(CaO); HMg=Halite(MgO); CZ=$CaZrO_3$.

4.4.2. Isothermal sections calculated for the ZrO_2–CaO–MgO system

The isothermal section calculated for the system between the temperatures 1420 and 1750 °C are very similar, so that only the 1420 and 1700 °C isothermal sections are presented (Figs. 5 and 6). The scant solubility of ZrO_2 in the Halite phases is clear when the limited extension of the compatibility field of $Halite_{MgO}$ and $Halite_{CaO}$ for all the isothermal sections is observed. In the system's rich-ZrO_2 region the calculated sections include the cubic-ZrO_2 and $CaZrO_3$ two-phase regions experimentally probed at 1600, 1700, and 1750 °C.[52]

Table 6
Calculated invariant point for the system ZrO_2–CaO–MgO

Invariant points	T (°C)	Fase	Phase composition (mol%)	
			ZrO_2	MgO
Eutectic: Liquid → Cubic + $Halite_{MgO}$ + $CaZrO_3$	2008	Liquid	46.95	28.43
		Cubic	74.31	11.21
		$Halite_{MgO}$	0.61	99.04
		$CaZrO_3$	50.00	0
Eutectic: Liquid → $Halite_{CaO}$ + $Halite_{MgO}$ + $CaZrO_3$	1982	Liquid	26.00	20.24
		$Halite_{CaO}$	1.67	10.66
		$Halite_{MgO}$	0.19	97.65
		$CaZrO_3$	50.00	0
Eutectic: Liquid → $Halite_{MgO}$ + $CaZrO_3$	2060	Liquid	37.03	26.13
		$Halite_{MgO}$	0.33	98.72
		$CaZrO_3$	50.00	0
Eutectoid: Cubic → Tetragonal + $Halite_{MgO}$ + ϕ_2	1054	Cubic	82.68	2.38
		Tetragonal	92.97	1.89
		$Halite_{MgO}$	0	99.99
		ϕ_2	76.00	–
Eutectoid: Tetragonal → Monoclinic + $Halite_{MgO}$ + ϕ_2	980	Tetragonal	93.08	2.31
		Monoclinic	100.00	–
		$Halite_{MgO}$	0	99.99
		ϕ_2	76.00	–
Decomposition: ϕ_2 → Cubic + $CaZrO_3$	1262	ϕ_2	76.00	–
		Cubic	79.07	3.00
		$CaZrO_3$	0.50	–

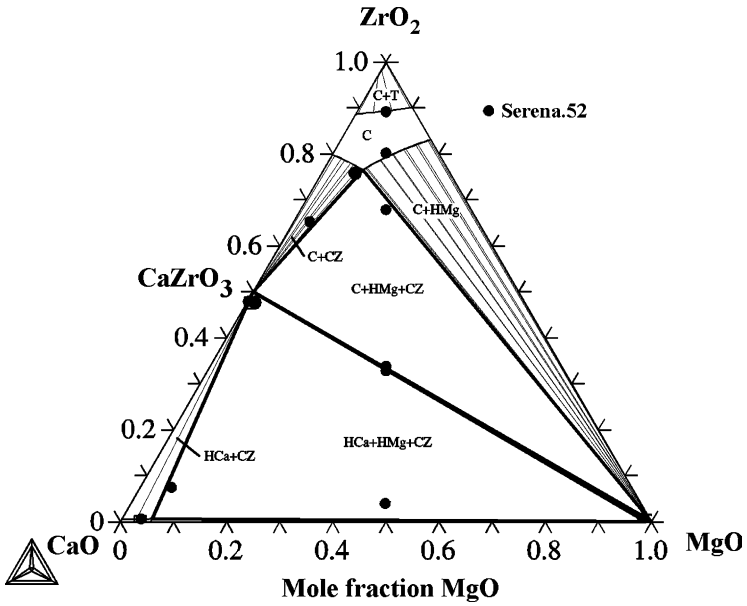

Fig. 6. The isothermal section at 1973 K of the optimized phase diagram ZrO_2–CaO–MgO. As comparison, the selected experimental data are also shown in the diagram. C=c–ZrO_2; T=t–ZrO_2; HCa=Halita(CaO); HMg=Halite(MgO); CZ=$CaZrO_3$.

The isothermal section calculated for 1420 °C (Fig. 4) is in good agreement with the experimental points reported by Yin and Arget[20] but not with those of Hellman and Stubican[17] for the boundaries of the tetragonal-ZrO_2 and cubic-ZrO_2 two-phase regions.

The isothermal sections of 1600–1750 °C are consistent with our own experimental data[52] as regards the extension of the different compatibility fields and the existence of the compatibility of the cubic-ZrO_2 and $CaZrO_3$ phases. The compositions of the cubic-ZrO_2 phase of the cubic-ZrO_2–$CaZrO_3$–MgO tie triangle calculated are also in line with the experimental results mentioned within experimental errors.

4.4.3. MgO–$CaZrO_3$ isoplethal section for the ZrO_2–CaO–MgO system

The MgO–$CaZrO_3$ isoplethal section calculated is shown in Fig. 7. In this section, the primary crystallization field

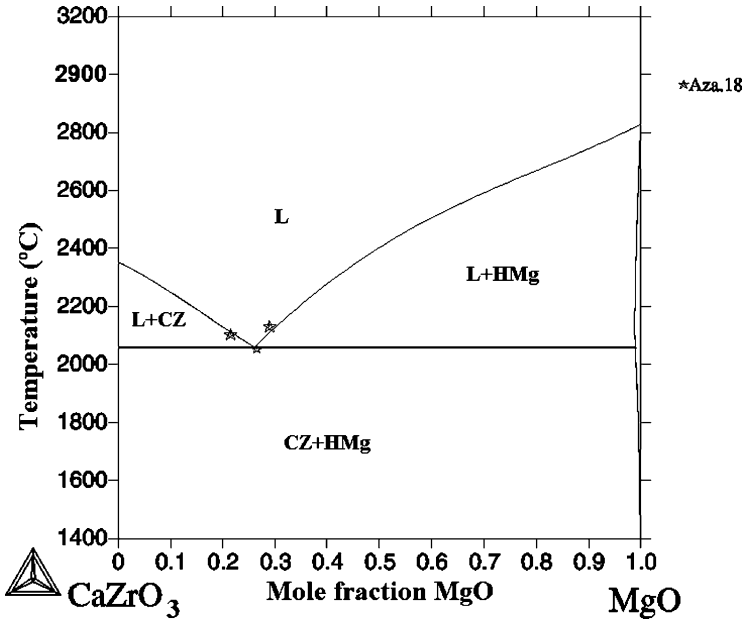

Fig. 7. The isoplethal section MgO–$CaZrO_3$ of the optimized phase diagram ZrO_2–CaO–MgO. As comparison, the selected experimental data are also shown in the diagram. L=Liquid; HMg=Halite(MgO) CZ=$CaZrO_3$.

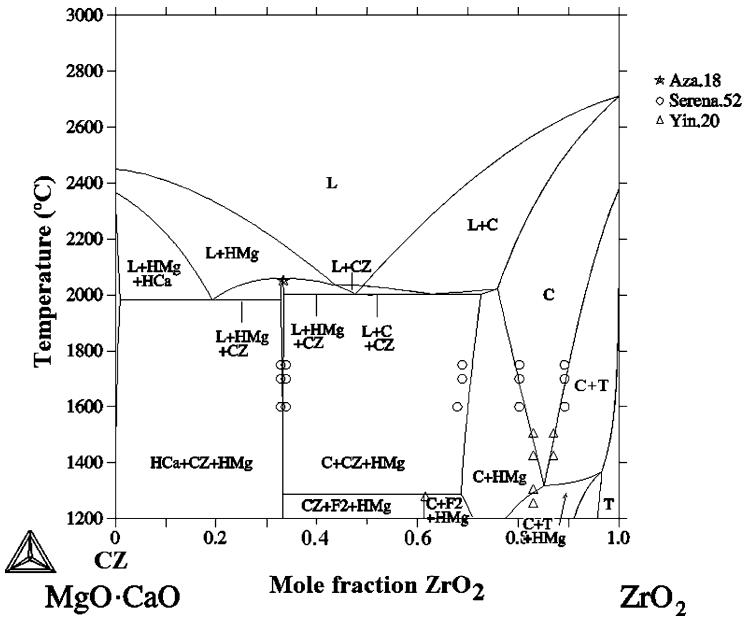

Fig. 8. The isoplethal section MgO·CaO–ZrO_2 of the optimized phase diagram ZrO_2–CaO–MgO. As comparison, the selected experimental data are also shown in the diagram. L=Liquid; C=c–ZrO_2; T=t–ZrO_2; M=m–ZrO_2; HCa=Halita(CaO); HMg=Halite(MgO); CZ=$CaZrO_3$; F2=$Ca_6Zr_{19}O_{44}$.

of the MgO and $CaZrO_3$ phases and the eutectic point are included. The liquidus surface is in accordance with the experimental data reported by de Aza et al.[18] for the invariant point of the pseudo-binary system. The small amount of solid solution existing in the MgO and the $CaZrO_3$ phases means that this section can be considered to be a simple binary system, with a eutectic point.

4.4.4. MgO·CaO–ZrO_2 isoplethal section for the ZrO_2–CaO–MgO system

Figs. 8 and 9 show the isoplethal section calculated for the ternary diagram erected on lines MgO·CaO–ZrO_2 in a general view and at lower temperatures, respectively. The superimposed experimental points make it possible to confirm the reasonable agreement existing between the isoplethal section calculated and the experimental information. The plane

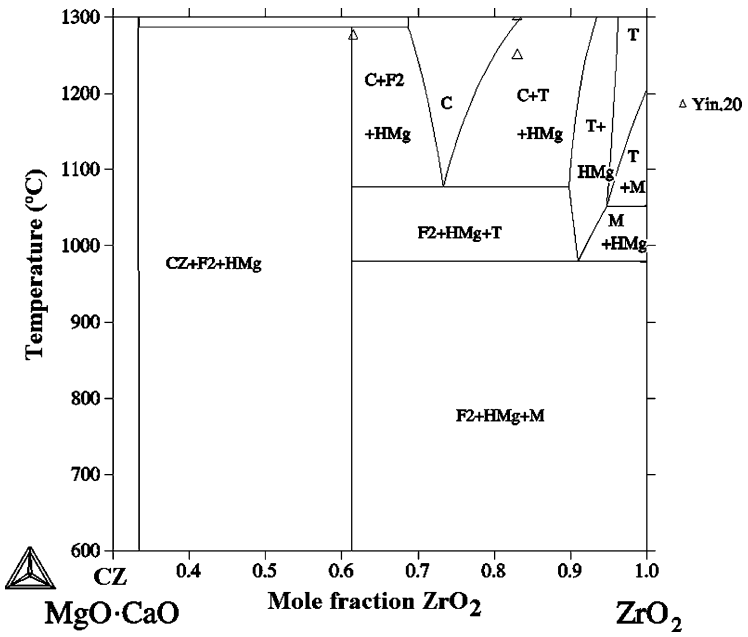

Fig. 9. The rich–ZrO_2 region of the isoplethal section MgO·CaO–ZrO_2 of the optimized phase diagram ZrO_2–CaO–MgO at lower temperatures. As comparison, the selected experimental data are also shown in the diagram. C=c–ZrO_2; T=t–ZrO_2; M=m–ZrO_2; HCa=Halita(CaO); HMg=Halite(MgO); CZ=$CaZrO_3$; F2=$Ca_6Zr_{19}O_{44}$.

of this isoplethal section intersects the field of primary crystallization of the cubic-ZrO_2, $CaZrO_3$, and MgO phases.

The isoplethal section intersects the MgO–$CaZrO_3$ subsystem showing the straight extension of the MgO and $CaZrO_3$ two-phase region. This field indicates the ratio of dolomite and ZrO_2 to be employed to obtain materials based on MgO and $CaZrO_3$.

The rich-ZrO_2 region, in the subsolidus includes the compatibility fields implied in the obtaining of partially and fully stabilized zirconia. The theoretical invariant subsolidus points calculated are shown in Table 6. The thermodynamic calculation allows a reasonable approximation of the rich-ZrO_2 region at lower temperatures to be obtained. This is *basically a theoretical assessment* because of the absence of experimental data for these temperatures, but the general aspect is "in accordance" with what is expected from the binary systems ZrO_2–CaO and ZrO_2–MgO.

5. Summary

An optimal set of thermodynamic functions for the binary systems MgO–CaO, ZrO_2–CaO, and ZrO_2–MgO was obtained from the selected phase diagram and thermodynamic data by using the Calphad technique. The comparison shows that the experimental information is reasonably well accounted for by the present description of the indicated binary systems.

The thermodynamic calculation of the ZrO_2–CaO–MgO ternary system was made from the binary calculated sides by using the Muggianu equation. The comparison for the liquidus surface and the isothermal and isoplethal sections calculated show that the experimental points are well reproduced by the calculation, within experimental uncertainty.

The MgO·CaO–ZrO_2 isoplethal section calculated at lower temperatures, has demonstrated that the present optimized parameters can provide insight into the thermodynamics in regions with scant or even no experimental information with some certainty.

It is hoped that the present phase diagram calculated will reduce and guide further experimental work in the ZrO_2–CaO–MgO system, especially at lower temperatures.

Acknowledgements

The authors wish to acknowledge financial support of the CICYT, Spain, under project number MAT-2000-0941 and by CAM project number CAM 07N/0038/2001.

References

1. Hannik, R. H. J., Kelly, P. M. and Muddle, B. C., Transformation toughening in zirconia containing ceramic. *J. Am. Ceram. Soc.* 2000, **83**(3), 461–487.
2. Bannister, M. J. and Garret, W. G., Production of stabilized zirconia for use as a solid-state electrolyte. *Ceram. Int.* 1975, **1**(3), 127–133.
3. Singhcl, S. G., Solid oxide fuel cells for stationary. *Solid State Ionics* 2002, **152/153**, 405–410.
4. Schmitt-Thomas, K. G. and Diet, U., Thermal barrier coatings with improved oxidation resistance. *Surf. Coatings Tech.* 1994, **68/69**, 113–115.
5. Betz, U. and Hahn, H., Ductibility of nanocrystalline zirconia based ceramic at low temperatures. *Nanostruct. Mater.* 1997, **9**, 717–726.
6. Betz, U., Sturn, A., Loeffler, J. F., Wagner, W., Wiedermann, A. and Hahn, H., Low-temperature isothermal sintering and microstructural characterization of nanocrystalline zirconia ceramic using small angle neutron scattering. *Nanostruct. Mater.* 1999, **12**, 689–926.
7. Chen, H., Zhou, X. and Ding, Ch., Investigation of the thermomechanical properties of a plasma-sprayed nanostructured zirconia coating. *J. Eur. Ceram. Soc.* 2003, **23**(9), 1449–1455.
8. Kaξpar, J. and Fornasiero, P., Nanostructured materials for advanced automotive de-pollution catalysts. *J. Solid State Chem.* 2003, **171**(1/2), 19–29.
9. Kaya, C., He, J. Y., Gu, X. and Butler, E. G., Nanostructured ceramic powders by hydrothermal synthesis and their applications. *Microporous Mesoporous Mater.* 2002, **54**, 37–49.
10. Mayo, M. J., High and low temperature superplasticity in nanocrystalline materials. *Nanostruct. Mater.* 1997, **9**, 717–726.
11. Suzuki, Y., Morgan, P. E. D. and Ohji, T., Synthesis and deformation behavior of nano-diphasic materials from natural dolomite. *Mat. Sci. Eng. A.* 2001, **304–306**, 780–784.
12. Suzuki, Y., Morgan, P. E. D. and Ohji, T., New uniformly porous $CaZrO_3$/MgO composites with three-dimensional network structure from natural dolomite. *J. Am. Ceram. Soc.* 2000, **83**(8), 2091–2093.
13. Corbitt, N., *Inorganic Membranes: Matkets, Technologies, Players*. Business Communication Co., Inc., Norwalk, 1997.
14. Chiang, Y., Wang, C. C. and Akbar, S. A., Calcium zirconate for the monitoring of hydrocarbons. *Sens. Actuators B* 1998, **46**, 208–212.
15. Suzuki, Y., Awano, M., Kondo, N. and Ohji, T., CH_4-sensing and high-temperature mechanical properties of porous $CaZrO_3$/MgO composites with three-dimensional network structure. *J. Ceram. Soc. Jpn.* 2001, **109**(1), 79–81.
16. Longo, V. and Podda, L., The phase diagram of the system ZrO_2–CaO–MgO between 1200 and 1700 °C. *Ceram. Int.* 1978, **4**(1), 21.
17. Hellman, J. R. and Stubican, V. S., Phase relations and ordering in the systems MgO–Y_2O_3–ZrO_2 and CaO–MgO–ZrO_2. *J. Am. Ceram. Soc.* 1983, **66**(4), 265–267.
18. de Aza, S., Richmond, C. and White, J., Compatibility relationships of Periclase in the system CaO–MgO–ZrO_2–SiO_2. *Trans. J. Br. Ceram. Soc.* 1974, **73**(4), 109–116.
19. Du, Y., Jin, Z. and Huang, P., Calculation of the ZrO_2–CaO–MgO phase diagram. *CALPHAD* 1992, **16**(3), 221–230.
20. Yin, Y. and Argent, B. B., The phase diagrams and thermodynamics of the ZrO_2–CaO–MgO and MgO–CaO systems. *J. Phase Equilibria* 1993, **14**(5), 588–600.
21. *Thermo-Calc Software Version p*. Stockholm, Sweden, 2003.
22. Rankin, G. A. and Merwin, H. E., The ternary system CaO–Al_2O_3–MgO. *J. Am. Chem. Soc.* 1916, **38**, 568.
23. Ruff, O., Ebert, F. and Krawczynski, U., Die Binare Systeme: MgO–CaO, MgO–BeO, CaO–BeO. *Z. Anorg. Allgem. Chem.* 1933, **213**(4), 333–335.
24. Von Wartenberg, H., Reusch, H. J. and Saran, E., Schmetz-diagramme höchstfeuurfester Oxyde: VII Systeme mit CaO und BeO. *Z. Anorg. Allgem. Chem.* 1937, **230**(3), 257–276.
25. Ford, W. F. and White, J., The CaO–MgO–Cr_2O_3 and CaO–MgO binary system. *Trans. Br. Ceram. Soc.* 1949, **48**(11), 417–427.
26. Doman, R. C., Barr, J. B., McNally, R. N. and Alper, A. M., Phase equilibria in the system CaO–MgO. *J. Am. Ceram. Soc.* 1963, **46**(7), 313.
27. Wu, P., Erickson, G. and Pelton, A. D., Critical evaluation and optimization of the thermodynamic properties and phase diagrams of

the CaO–FeO, CaO–MgO, CaO–MnO, FeO–MgO, FeO–MnO and MgO–MnO systems. *J. Am. Ceram. Soc.* 1993, **76**(8), 2065–2075.
28. Tepesch, P. D., Kohan, A. E., Garbulsky, G. D. and Ceder, G., A model to compute phase diagrams in oxides with empirical or first-principles energy methods and application to the solubility limits in the CaO–MgO system. *J. Am. Ceram. Soc.* 1996, **79**(8), 2033–2040.
29. Longo, V. and Podda, L., The phase diagram of the system ZrO_2–CaO–MgO between 1200 and 1700 °C. *Ceram. Int.* 1978, **4**(1), 21.
30. Henney, J. W. and Jones, J. W., *Trans. Br. Ceram. Soc.* 1969, **68**, 201.
31. Du, Y., Jin, Z. and Huang, P., Thermodynamic calculation of the zirconia-calcia system. *J. Am. Ceram. Soc.* 1992, **75**(11), 3040–3048.
32. Hellman, J. R. and Stubican, V. S., The existence and stability of $Ca_6Zr_{19}O_{44}$ in the system ZrO_2–CaO. *Mat. Res. Bull.* 1982, **17**, 459–465.
33. Yin, Y. and Argent, B. B., Phase diagrams and thermodynamics of the system ZrO_2–CaO and ZrO_2–MgO. *J. Phase Equilibria* 1993, **14**(4), 439–450.
34. Stubican, V. S. and Ray, S. P., Phase equilibria and ordering in the system ZrO_2–CaO. *J. Am. Ceram. Soc.* 1977, **60**(11/12), 534–537.
35. Traverse, J. P. and Foex, M., Zirconia–strontia and zirconia–lime system. *High Temp. High Pressure* 1969, **1**(4), 409–427.
36. Noguchi, T., Mizuno, M. and Conn, W. M., Fundamental research in the refractory system with a solar furnace-zirconium dioxide–calcium oxide system. *Sol. Energy* 1967, **11**(3/4), 145–152.
37. Garvie, R. C., The cubic field in the system CaO–ZrO_2. *J. Am. Ceram. Soc.* 1968, **68**(10), 553–556.
38. Stringer, R. K., The cubic–tetragonal phase boundary in the calcia–zirconia system. *Proc. Aust. Ceram. Conf.*, 1978, **8**, 128–134.
39. Duran, P., Recio, P. and Rodriguez, J. M., Low temperature phase equilibria and ordering in the ZrO_2-rich region of the system zirconia–calcia. *J. Mater. Sci.* 1987, **22**(12), 4348–4356.
40. Strickler, D. W. and Carlson, W. G., Ionic conductivity of cubic solid solutions in the system CaO–Y_2O_3–ZrO_2. *J. Am. Ceram. Soc.* 1964, **47**(3), 122–127.
41. Cocco, A., Composition limits at high temperatures of the cubic phase composed of ZrO_2 and CaO. *Chim. Ind. (Milan)* 1959, **41**(9), 882–886.
42. Tien, T. Y. and Subbarao, E. C., X-ray and electrical conductivity study of the fluorite phase in the system ZrO_2–CaO. *J. Chem. Phys.* 1963, **39**(4), 1041–1047.
43. Nishimo, T., Estimation of a portion of the phase diagram in the calcium oxide–zirconium dioxide system by reacting $CaZrO_3$ with Cr_2O_3. *Nippon Kagaku Kaishi* 1981, **10**, 1681–1683.
44. Grain, C. F., Phase relation in the ZrO_2–MgO system. *J. Am. Ceram. Soc.* 1967, **50**(6), 288–290.
45. Delamarre, C., Existence and structure of a new compound of formula M_7O_{12} in zirconia–magnesia and hafnia–magnesia systems. *C. R. Hedb. Seances Acad. Sci. Ser. C* 1965, **269**, 113–115.
46. Hannink, R. H. J. and Garvie, R. C., Subeutectoid aged Mg–PSZ alloy with enhanced thermal up-shock resistance. *J. Mater. Sci.* 1982, **17**, 2637–2643.
47. Sim, S. M. and Stubican, V. S., Phase relations and ordering in the system MgO–ZrO_2. *J. Am. Ceram. Soc.* 1987, **70**(7), 521–526.
48. Zhirnova, N. A., *Zhur. Priklad. Khim.* 1939, **12**, 1279.
49. Ebert, F. and Cohn, E., System ZrO_2–MgO. *Z. Anorg. Allgem. Chem.* 1933, **213**, 321–322.
50. Duran, P., Rodriguez, J. M. and Recio, P., The ZrO_2-region of the ZrO_2–MgO system. *J. Mater. Sci.* 1991, **26**, 467–472.
51. Muggianu, Y. M., Gambino, M. and Bross, J. P., *J. Chim. Phys.* 1975, **22**, 83.
52. Serena, S., Sainz, M. A., Caballero A., Experimental determination and thermodynamic calculation of the ZrO_2–CaO–MgO phase equilibria diagram. Isothermal sections at 1600, 1700, and 1750 °C, in press.
53. *Oxunary Data Banck*, compiled by Dinsdale, N.P.L. Teddington, UK, 1997.